Journal of Magnetism and Magnetic Materials 321 (2009) 3712–3718

Contents lists available at ScienceDirect

Journal of Magnetism and Magnetic Materials

journal homepage: www.elsevier.com/locate/jmmm

Radio-frequency measurements of UNiX compounds (X = Al, Ga, Ge) in high magnetic fields

A.M. Alsmadi [a,*], S. Alyones [a], C.H. Mielke [b], R.D. McDonald [b], V. Zapf [b], M.M. Altarawneh [b], A. Lacerda [b], S. Chang [c], S. Adak [d], K. Kothapalli [d], H. Nakotte [d]

[a] Physics Department, The Hashemite University, 13115 Zarqa, Jordan
[b] National High Magnetic Field Laboratory, Pulsed Field Facility, Los Alamos National Laboratory, Los Alamos, NM 87545, USA
[c] NIST Center for Neutron Research, National Institute of Standards and Technology, Gaithersburg, MD 20899, USA
[d] Physics Department, New Mexico State University, Las Cruces, NM 88003, USA

ARTICLE INFO

Article history:
Received 15 March 2009
Received in revised form
13 June 2009
Available online 16 July 2009

Keywords:
Uranium compounds
Complex conductivity
Metamagnetic transition

ABSTRACT

We performed radio-frequency (RF) skin-depth measurements of antiferromagnetic UNiX compounds (X = Al, Ga, Ge) in magnetic fields up to 60 T and at temperatures between 1.4 to ~60 K. Magnetic fields are applied along different crystallographic directions and RF penetration-depth was measured using a tunnel-diode oscillator (TDO) circuit. The sample is coupled to the inductive element of a TDO resonant tank circuit, and the shift in the resonant frequency Δf of the circuit is measured. The UNiX compounds exhibit field-induced magnetic transitions at low temperatures, and those transitions are accompanied by a drastic change in Δf. The results of our skin-depth measurements were compared with previously published B–T phase diagrams for these three compounds.

1. Introduction

Uranium compounds have been the subject of many studies in the past decades due to interest in the specific nature of U 5f-electron magnetism. The 5f electrons of U are found to be intermediate between the delocalized d electrons of the transition metals and the well-localized 4f electrons of the lanthanides. For uranium compounds, there are two mechanisms that lead to the delocalization the 5f electrons: the direct 5f–5f overlap and the 5f-ligand hybridization [1]. However, while 5f-ligand hybridization can cause delocalization of the 5f states (suppression of 5f moments), it can also mediate indirect exchange interaction between them and thus promote long-range magnetic order. Another striking feature of uranium compounds is the huge magnetocrystalline anisotropy, and hybridization effects are again believed to play a key role in its origin.

Ternary UTX intermetallic compounds (U = Uranium, T = transition metal, and X = p-electron element) provide a rich system for the study of the role of the 5f-ligand hybridization and the formation of the uranium magnetic moments [1,2]. UTX compounds were found to crystallize mainly in four different crystal structures: the cubic MgAgAs, the hexagonal Fe_2P, the hexagonal $CaIn_2$ and the orthorhombic $CeCu_2$ structures or its ordered variants [2]. The formation of a specific structure seems to be connected with the number of d electrons in the transition metal [3]. The two largest groups of isostructural compounds are those with the hexagonal Fe_2P (ordered variant: ZrNiAl)-type and the orthorhombic $CeCu_2$ (ordered variant: TiNiSi)-type of structure. For X = Si or Ge, the $CeCu_2$ (or TiNiSi) structure is obtained, whereas most of the compounds with larger X atoms, such as Al and Ga, typically crystallize in the ZrNiAl-type structure [4,5].

Systematic studies of UTX compounds have provided some general trends for the development of magnetism of UTX compounds, e.g., for the size of magnetic 5f moment [3]. However, there is still limited understanding about the main mechanisms that are responsible for the formation of the (often complex) magnetic structures and (often multiple) magnetic transitions between different phases of these materials.

Magnetic structures arise from the balance of interactions that are influenced by thermodynamic parameters such as temperature, external pressure and magnetic fields. This paper deals with UTX compounds that have an antiferromagnetic ground state. The study of field-induced magnetic transitions in antiferromagnets can provide some insight into the strength of exchange interactions. It is common to refer to field-induced transitions as metamagnetic transitions, in analogy to the metastable (metamagnetic) state that is induced above a critical field, B_C. Metamagnetic transitions take place in a magnetic field sufficient to overcome the antiferromagnetic interactions and to modify the magnetic structure. The change in the magnetic structure is often connected with a change of the translational symmetry, and is usually accompanied by a noticeable change in the magnetore-

* Corresponding author.
E-mail address: alsmadi_abd@yahoo.com (A.M. Alsmadi).

0304-8853/$ - see front matter © 2009 Elsevier B.V. All rights reserved.
doi:10.1016/j.jmmm.2009.07.022

sistance [1]. As mentioned above, the magnetic anisotropy in uranium compounds is huge, and metamagnetic transitions in these compounds often occur in the 10–60 T range [1], which is generally accessible only with the use of pulsed magnetic fields. There are technological challenges for magnetoresistance studies in pulsed fields, such as pick-up of induced electronic noise in leads, integrity of resistance contacts and their contact resistance, eddy-current effects, and magnetic torque (rotation) effects of the sample during the field pulse.

Here, we present an alternative to magnetoresistance studies using a contactless conductivity measurement technique that overcomes many of the above mentioned drawbacks. The radio-frequency (RF) skin-depth technique is a very useful probe of magnetotransport since the skin depth of the sample can be related to its complex conductivity, which can be converted to its resistivity [6–8]. Unlike magnetoresistance, RF skin-depth is a non-contact technique that measures changes in the mutual inductance between the sample and a coil that is resonated at high frequencies via a tunnel-diode oscillator (TDO) tank circuit. The RF technique is a relatively new technique, and it has been used mostly for measurements on semi-conductors and insulators, such as high-T_C superconductors [7]. Recently, however, it was successfully used in metallic samples [8] and on doped insulators that show metallic behavior [9]. Our preliminary results for UNiAl, UNiGa and UNiGe [10] have proven that RF skin-depth measurements can be used for the essentially metallic UTX compounds as well. In particular, we found a direct correspondence between the features in RF measurements and magnetoresistance [10]. However, our previous studies were done only at liquid-helium temperature with the magnetic field applied only along the easy-axis direction(s).

Here, we present measurements of the radio-frequency (RF) skin-depth for antiferromagnetic UNiX (T = Ni, and X = Al, Ga, Ge) in magnetic fields up to 60 T, applied along different crystallographic directions for a wide range of temperatures. In Table 1 we summarize the crystal structure, the ordering temperatures, T_N, and transition fields, B_C for antiferromagnetic UNiX compounds presented in these studies.

2. Experimental

The experiments were performed on single crystals using the 60 T short-pulse magnet at the pulsed field facility, NHMFL, Los Alamos National Laboratory. The experiments were performed on the same crystals used in the previous study [10]. Bar-shaped sample (typically $0.5 \times 0.5 \times 4\,mm^3$) were cut parallel and perpendicular to the easy-magnetization directions.

The radio-freqency (RF) skin-depth measurements were done using a tunnel-diode oscillator (TDO) with a resonance frequency

$$f = 1/2\pi\sqrt{LC} \tag{1}$$

the TDO is an RF tank-circuit oscillator, for which the losses in the LC circuit are compensated by the bias on the tunnel diode in the negative resistance region of its I–V characteristic [11]. Cryogenic temperatures are necessary to provide a large enough negative resistance to cause the tank circuit to oscillate. In the TDO method, the RF skin depth is measured by coupling the sample to the coil of the tank circuit and measuring the shift in the resonant frequency. When a magnetic sample is inserted into a tank coil, the inductance L is shifted by a small amount ΔL, which is proportional to the a.c. susceptibility χ. As a result, the resonance frequency is shifted by Δf according to the relation

$$\frac{\Delta f}{f} = -\frac{\Delta L}{2L} \tag{2}$$

the shift in the resonance frequency Δf is related to the resistivity ρ for metallic samples through the skin depth

$$\delta = \sqrt{\rho/\pi\mu_0 f} \tag{3}$$

where μ_0 is the permittivity of free space. The change of resonance frequency is related to the shift in the skin depth as

$$\frac{\Delta f}{f} = -\frac{G\Delta\delta}{\delta} \tag{4}$$

where G is the geometrical factor that depends on the sample and the coil geometries [7,8]. In our measurements, we used output frequency of about 1 MHz at zero magnetic field.

The RF skin-depth measurements are commonly referred to as complex-conductivity measurements in the literature. The frequency (and amplitude) shifts reflect the change in both the real and imaginary components of the conductivity. So this technique is sensitive to the dielectric (permittivity: ε_r) and the magnetic (permeability:μ_r) material properties. This technique has a high sensitivity of the order of 1 part in 10^9, and the experimental setup is relatively simple, and the non-contact method avoids damage to the sample or heating due to the leads. A more detailed description of the experimental set up used in the studies presented here is discussed in Ref. [7].

Table 1
Crystal structures, ordering temperatures, T_N, and transition field(s), B_C, for UNiX compounds (X = Al, Ga and Ge) [1].

Compound	*Crystal structure*	T_N (K)	B_C (T)
UNiAl	Hexagonal ZrNiAl	19.3	11.1
UNiGa	Hexagonal ZrNiAl	34.1[a]	0.4–0.9
UNiGe	Orthorhombic TiNiSi	41.5	17 and 25 (*b*-axis) 3 and 10 (*c*-axis)

[a] Three other transitions occur at slightly higher temperatures below 40 K.

3. Results and discussion

We performed RF measurements on three antiferromagnetic UNiX compounds: the hexagonal ZrNiAl-type compounds, UNiAl and UNiGa, and the orthorhombic TiNiSi-type compound, UNiGe.

3.1. UNiAl

UNiAl crystallizes in the hexagonal ZrNiAl-type structure [1]. UNiAl is best described as an itinerant 5f-electron antiferromagnet (AF) with $T_N = 19.3$ K [1]. Single-crystal studies reveal that UNiAl exhibits a large magnetic anisotropy with the easy-magnetization direction along the hexagonal c-axis [12–15] and it can be classified as a moderate heavy-fermion system since an electronic contribution to the low-temperature specific heat of $\gamma = 164\,mJ/mol\,K^2$ was reported [16–18]. At low temperatures, this compound undergoes a metamagnetic transition for the magnetic field along c-axis, and the critical field was found to be equal to $B_C = 11.35$ T at 1.7 K [14].

Fig. 1 displays the anisotropic behavior of the measured relative frequency shift of the tank circuit $\Delta f/f_{B=0}$ for UNiAl as a function of applied magnetic fields at 1.5 K. When the field is applied along the c-axis, we observe a sudden reduction in $\Delta f/f_{B=0}$ at $B_C = 11.1$ T. For fields applied perpendicular to the c-axis, there is no similar transition, but just a smooth and continuous decrease in $\Delta f/f_{B=0}$. This anisotropic behavior in $\Delta f/f_{B=0}$ is consistent with the magnetic anisotropy reported from previous bulk studies on single-crystalline UNiAl [14].

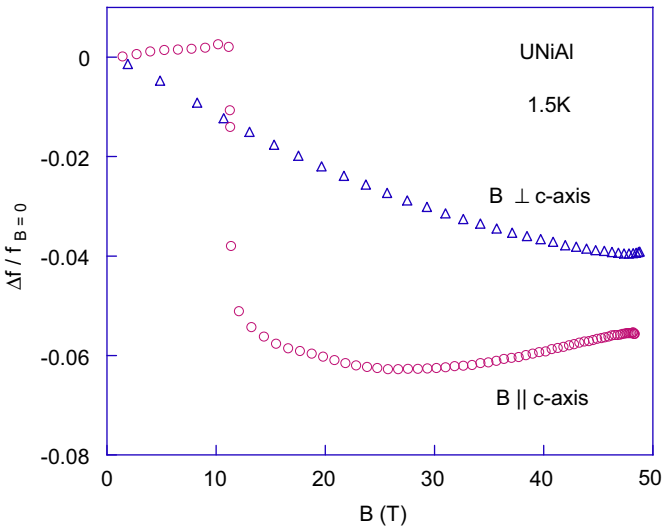

Fig. 1. Field dependence of the relative frequency shift $\Delta f/f_{B=0}$ of the resonant tank-circuit oscillations for UNiAl at 1.5 K with fields applied along (circles) and perpendicular to (triangles) the c-axis. For $B\|c$-axis, we observed a metamagnetic transition around $B_C = 11.1$ T, while no such transition is seen for fields up to 50 T for $B\perp c$-axis. Errors are smaller than the symbols.

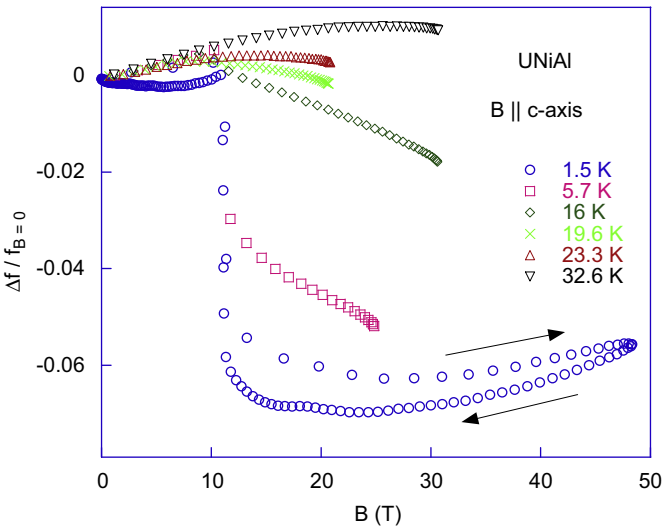

Fig. 2. Field dependence of the relative frequency shift $\Delta f/f_{B=0}$ of the tank-circuit oscillations for UNiAl with fields applied along the c-axis at different temperatures. At 1.5 K, the frequency shift for both the up- and down-sweeps of the pulsed field is shown. For higher temperatures, only the results from up-sweeps are shown.

Fig. 2 shows the field dependence of the measured relative frequency shift $\Delta f/f_{B=0}$ in UNiAl at different temperatures for fields applied along the c-axis. The frequency shift for up- and down-sweeps of the field is shown only for $T = 1.5$ K, while for other temperatures only the results from up-sweeps are shown. The up-sweep is much faster than the down-sweep, so the temperature is more accurate on the up-sweep since the sample has not had enough time to heat. The transition at 1.5 K exhibits a very narrow hysteresis around the transition field (~0.06 T at 1.5 K) in $\Delta f/f_{B=0}$. The hysteresis around B_C is believed to be real and it has been observed previously [19]. In contrast, the differences in the values for $\Delta f/f_{B=0}$ above B_C are a function of dB/dt and the maximum applied field, and we tentatively attribute those to eddy-current heating during the field pulse. With increasing temperatures, the metamagnetic transition from the antiferromagnetic state towards a field-induced ferromagnetically-aligned phase at $B_C = 11.1$ T is shifted to lower fields, in good agreement with previous results [14]. The metamagnetic transition disappears for temperatures above the Néel temperature, $T_N = 19.3$ K, but we still observe a change in the slope of $\Delta f/f_{B=0}$ even at temperatures well above T_N, e.g. a change in the slope of $\Delta f/f_{B=0}$ at $T = 32.6$ K at field about 25 T. This behavior is consistent with previously reported large magnetoresistance effects above T_N in UNiAl [19,20]. In general, the magnetoresistance response in UNiAl and many other uranium compounds has been attributed to the suppression of AF fluctuations and to the disappearance of the magnetic superzones when the AF ordering is suppressed by magnetic field [14,21,22].

As we discussed before in the experimental part, shifts in the resonant frequency, Δf, is proportional to the normal skin depth of the sample, δ. Using simple geometrical relations and estimates for sample dimensions in the current experiments, the resistivity can be related to the frequency shift as

$$\rho = \left(\frac{R^2}{r_s}\frac{\Delta f}{f_0}\sqrt{\mu_0\pi f} + \delta_0\sqrt{\mu_0\pi f}\right)^2 \quad (5)$$

where R is the effective radius of the coil, r_s the effective sample radius, μ_0 the permittivity of free space, f_0 the resonant frequency at $B = 0$, and δ_0 the skin depth at $B = 0$. In order to relate the

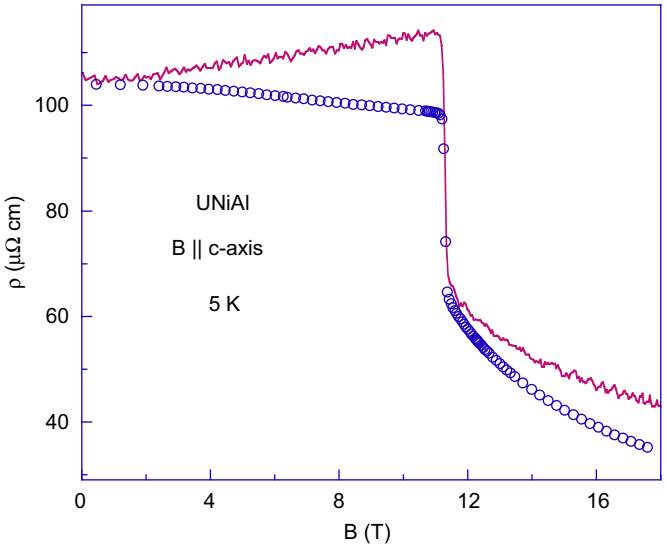

Fig. 3. Field dependence of the electrical resistivity of the UNiAl at 5 K, with $B\|c$-axis. The previously measured resistivity data (open circles) are taken from Ref. [15]. The solid line represents the calculated resistivity based on our frequency shift measurements.

measured changes in the frequency Δf with previously measured resistivity [15], the measured resistivity data and the calculated resistivity using Eq. (4) and our frequency shift measurements as a function of applied magnetic field along the crystallographic c-axis of UNiAl are shown in Fig. 3. In this case, the measured resistivity (open circles) is in good agreement with the calculated resistivity (solid line) based on our frequency shift measurements.

We took the anomalies in the measured relative frequency shift $\Delta f/f_{B=0}$ to extract the critical fields for the B–T magnetic phase diagram for $B\|c$-axis in UNiAl. The results are shown as solid circles in Fig. 4, which depicts the B–T phase diagram of UNiAl for fields applied along the c-axis. Fig. 4 also contains the metamagnetic transition fields, B_C, determined from the anomalies of our $\Delta f/f_{B=0}$ data, together with the results from previously reported specific heat [14], magnetization [14] and magnetoresistance [19] studies. For UNiAl, the boundary of the

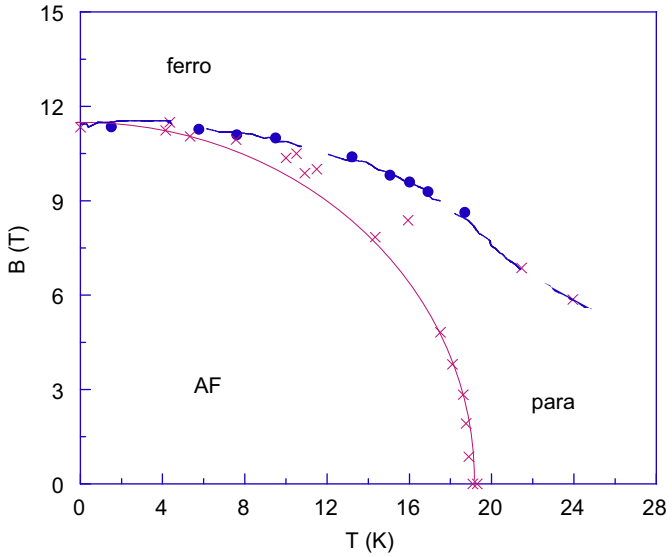

Fig. 4. Magnetic B–T phase diagram of UNiAl for field applied along the c-axis. Solid circles are taken from the anomalies of the relative frequency shift $\Delta f/f_{B=0}$ of the tank circuit, while crosses are the results from previously published data from specific heat and magnetoresistance studies [17]. The magnetic phases are labeled 'AF' for the antiferromagnetic phase, 'ferro' for the field-induced ferromagnetically-aligned phase and 'para' for the paramagnetic phase. Lines are guides to the eye. The boundary of the antiferromagnetic phase was established by specific-heat experiments in applied magnetic fields (solid line), but short-range magnetic correlations persist well above T_N (dashed line).

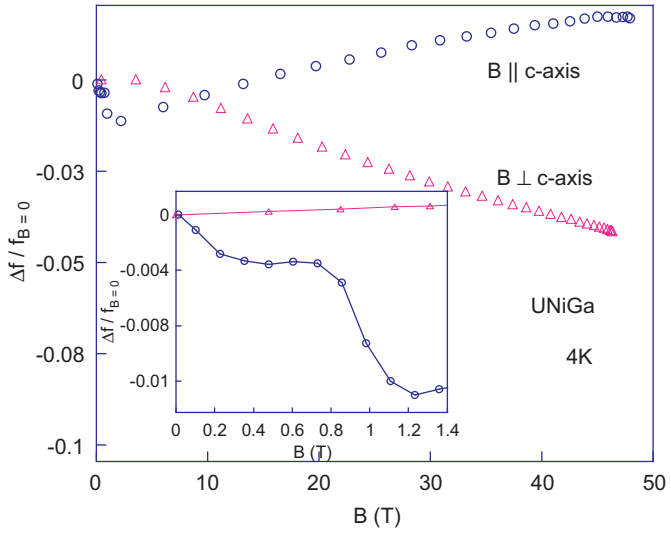

Fig. 5. Field dependence of the relative frequency shift $\Delta f/f_{B=0}$ of the resonant tank-circuit oscillations for UNiGa at 4 K with fields applied along (circles) and perpendicular to the c-axis (triangles). For $B\|c$-axis, we observed a slight change of slope at 0.25 T and a metamagnetic transition near $B_C = 0.85$ T, while no transition up to 50 T is found for $B\perp c$ axis. The inset shows the low-field response for $B\|c$-axis.

antiferromagnetic phase was established by specific-heat experiments in applied magnetic fields (solid line in Fig. 4). However, magnetic and magnetoresistance results studies had revealed that short-range magnetic correlations persist well above T_N, and the inflection points of the magnetic isotherms occur well above the boundary when approaching T_N (dashed line in Fig. 4). The B_C values determined from the anomalies in the measured relative frequency shift, $\Delta f/f_{B=0}$, are consistent with the B_C values determined from the inflection points of the magnetic isotherms and the results are in excellent agreement with the previously reported B–T phase diagram [14].

3.2. UNiGa

UNiGa is another UTX compound that crystallizes in the hexagonal ZrNiAl-type structure [1]. It shows a very complex magnetic phase diagram where multiple antiferromagnetic transitions are found between 35 and 40 K [23–29]. For all magnetic phases, the strong uniaxial anisotropy keeps the moments aligned along the c-axis. A relatively low magnetic field of less than 1 T applied along the c-axis induces metamagnetic transitions from the zero-field antiferromagnetic structures to uncompensated antiferromagnetic or a ferromagnetically-aligned phase.

Probably the most prominent and discussed feature in UNiGa is the large reduction of the electrical resistivity at the metamagnetic transition, especially for the current along c-axis where $\Delta\rho/\rho(0T) = 86\%$ [30]. Subsequently, we expect to observe a drastic change also in the frequency shift (Δf) at the metamagnetic transition in UNiGa.

Fig. 5 displays the anisotropic behavior of the measured relative frequency shift of the tank circuit $\Delta f/f_{B=0}$ for UNiGa as a function of applied magnetic fields at 4 K. Similar to UNiAl, application of a magnetic field has only a small effect on $\Delta f/f_{B=0}$ for $B\perp c$-axis, while there is a strong dependence when the field is applied along the c-axis. At 4 K, for fields applied along the c-axis, we observed a slight change in the slope of $\Delta f/f_{B=0}$ at 0.25 T and a sudden reduction in the relative frequency shift (~1% of its zero-field value) at $B_C = 0.88$ T (see inset of Fig. 4). The anisotropic behavior of $\Delta f/f_{B=0}$ for UNiGa is consistent with the magnetic anisotropy reported from previous single-crystal studies [23–29].

Fig. 6 shows the field dependence of the relative frequency shift of the tank circuit $\Delta f/f_{B=0}$ of UNiGa for fields applied along the c-axis at different temperatures. At 4 K, the change in the slope of $\Delta f/f_{B=0}$ at 0.25 T and the metamagnetic transition at $B_C = 0.88$ T move toward each other, join for temperatures around 20 K, and then split again for higher temperatures.

Taking all the anomalies in measured relative frequency shift in the tank circuit, $\Delta f/f_{B=0}$, we extracted the critical field for $B\|c$-axis and show the resulting B–T phase diagram together with previously published data for UNiGa from magnetic and neutron-diffraction results [25–29]. The phase diagram is shown in Fig. 7. Clearly, our results are again in good agreement with previous data.

3.3. UNiGe

UNiGe crystallizes in the orthorhombic TiNiSi-type structure [1]. Unlike UTX compounds crystallizing in the hexagonal ZrNiAl structure, which exhibit strong uniaxial anisotropy, a variety of moment configurations are observed for different UTX compounds crystallizing in TiNiSi structure [1]. This indicates that the balance of exchange interactions is more delicate in compounds with this structure than those with the ZrNiAl structure.

Bulk and neutron-diffraction studies on UNiGe indicated two antiferromagnetic transitions at about 42 and 50 K [31–38]. High-field magnetization measurements [34] showed that there are two metamagnetic transitions in UNiGe for field applied along c-axis (at 3 and 10 T) and two transitions with field along the b-axis (at 17 and 25 T). For the a-axis, the magnetization curve at 4.2 K is linear up to 38 T and the response is much weaker. Similar to other UTX compounds, UNiGe shows a huge magnetic anisotropy. However, this compound is exceptional because it is unusual to find that the 5f moments have a significant component along the hard direction, which is contrary to expectations based on the

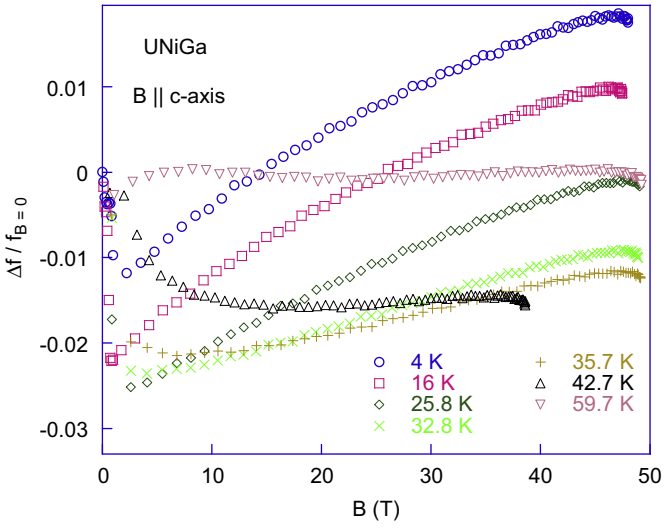

Fig. 6. Field dependence of the relative frequency shift $\Delta f/f_{B=0}$ of the tank-circuit oscillations for UNiGa with fields applied along the *c*-axis at different temperatures. Only field up-sweeps are shown.

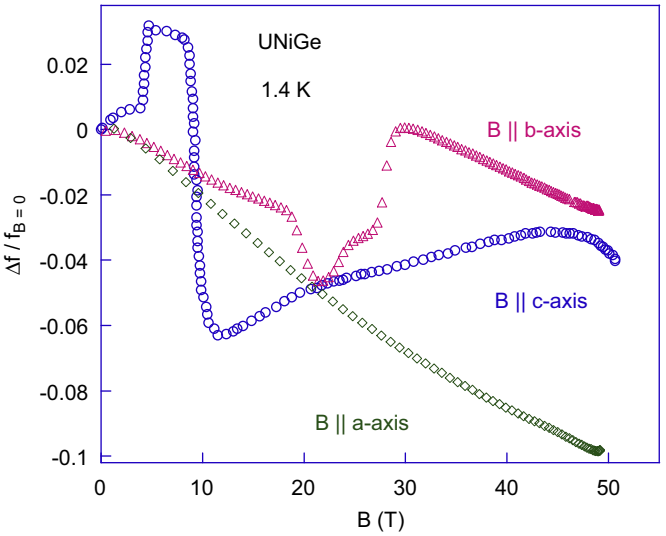

Fig. 8. Field dependence of the relative frequency shift $\Delta f/f_{B=0}$ of the resonant tank-circuit oscillations for UNiGe at 1.4 K with magnetic fields applied along *a*, *b* and *c*-axes, represented by diamonds, triangles and circles, respectively.

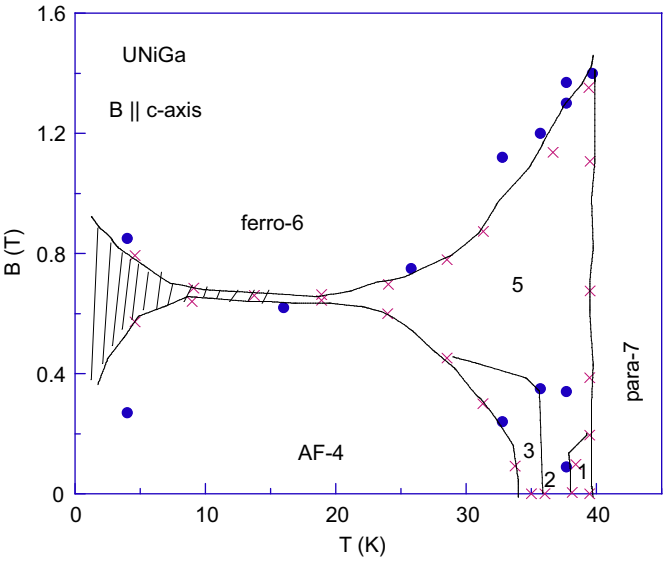

Fig. 7. Magnetic *B*-*T* phase diagram of UNiGa for field applied parallel to the *c*-axis. Solid circles are taken from the anomalies in the measured relative frequency shift $\Delta f/f_{B=0}$ in the tank circuit, and crosses represent previously published results from bulk magnetic and neutron-diffraction experiments [26]. The magnetic phases are labeled; '1' for incommensurate antiferromagnetic (AF) structure with a magnetic propagation vector $q \approx (0,0,0.36)$, '2' for an AF phase with $q = (0,0,1/3)$, '3' for an AF phase with $q = (0,0,1/8)$, 'AF-4' for the ground- state AF phase with $q = (0,0,1/6)$, '5' for the uncompensated antiferromagnetic phase with $q = (0,0,1/3)$, 'ferro-6' for the field-induced ferromagnetic phase with $q = (0,0,0)$, and 'para-7' for the paramagnetic phase. The shaded area represents a region where hysteresis effects occur. The lines are guides to the eye.

models involving single-ion anisotropies of different sublattices [39].

Fig. 8 displays the anisotropic behavior of the measured relative frequency shift in the tank circuit $\Delta f/f_{B=0}$ of UNiGe as a function of applied magnetic fields at 1.4 K. For fields applied along the *b*-axis, our RF measurements reveal three anomalies at 18, 24 and 28 T in the field up-sweep. For fields applied along the *c*-axis, two metamagnetic transitions were observed at 4.5 and 9.5 T in the field up-sweep. These results had been reported previously [40], but no comparison with *B*–*T* phase boundaries was done. For fields applied along the *a*-axis, on the other hand, only a smooth and continuous decrease in $\Delta f/f_{B=0}$ is observed, indicating that the *a*-axis is the hard axis in UNiGe. The anisotropic response in $\Delta f/f_{B=0}$ for UNiGe is again consistent with the magnetic anisotropy inferred from previous single-crystal studies [34,35].

Fig. 9 shows the relative frequency shift of the tank circuit $\Delta f/f_{B=0}$ for UNiGe at various temperatures for fields applied along the *b*-axis (Fig. 9a) and the *c*-axis (Fig. 9b). For both orientations only the lowest critical fields (at 1.4 K, $B_C = 18$ T for $B \| b$-axis and $B_C = 4.5$ T for $B \| c$-axis) exhibit a strong suppression with increasing temperature, while the transitions at higher fields remain relatively flat up to ~35 K.

For $B \| b$-axis, only two transitions around 17 and 25 T were reported previously from magnetoresistance measurements [34], while there was no report of a third transition. Since our sample was different than the one from Ref. [34], we decided to check whether the occurrence of a third metamagnetic transition could be attributed to different quality of the two samples or whether it might be an intrinsic property. We repeated the magnetoresistance measurement for $B \| b$-axis on our sample, which was used for RF skin-depth study. The symbols in Fig. 10 show the measured resistivity of UNiGe as a function of magnetic fields applied along the *b*-axis for our sample. At 4 K, the resistivity exhibits only two clear metamagnetic transitions at 18.5 and 26 T, in agreement with previous reports [34], while $\Delta f/f_{B=0}$ seems to show three transitions (see Fig. 9a).

Moreover, we find an increase in $\Delta f/f_{B=0}$ at 24 and 28 T but a decrease in the resistivity at ~26 T. The different sign in the RF skin depth and the magnetoresistance response is unlike the behavior for $B \| c$-axis in UNiGe, where signs in the RF skin depth and the magnetoresistance are the same at both transition fields, as is also the case for UNiAl and UNiGa [10], i.e. the frequency shift mirrors the magnetoresistance. In fact, using Eq. (5), we computed the resistivity based on our frequency shift measurements (solid line in Fig. 10). Clearly, we observed a marked deviation for the behavior of these two properties. The different behavior of $\Delta f/f_{B=0}$ and the resistivity (or $\Delta\rho/\rho_{B=0}$) may not be too surprising because the frequency shift is sensitive to both the dielectric and magnetic properties, and it is conceivable that for particular field orientations the effects can be additive and while for other orientations the signs could be opposite [10]. The properties which are dominant depend on many factors, such as the

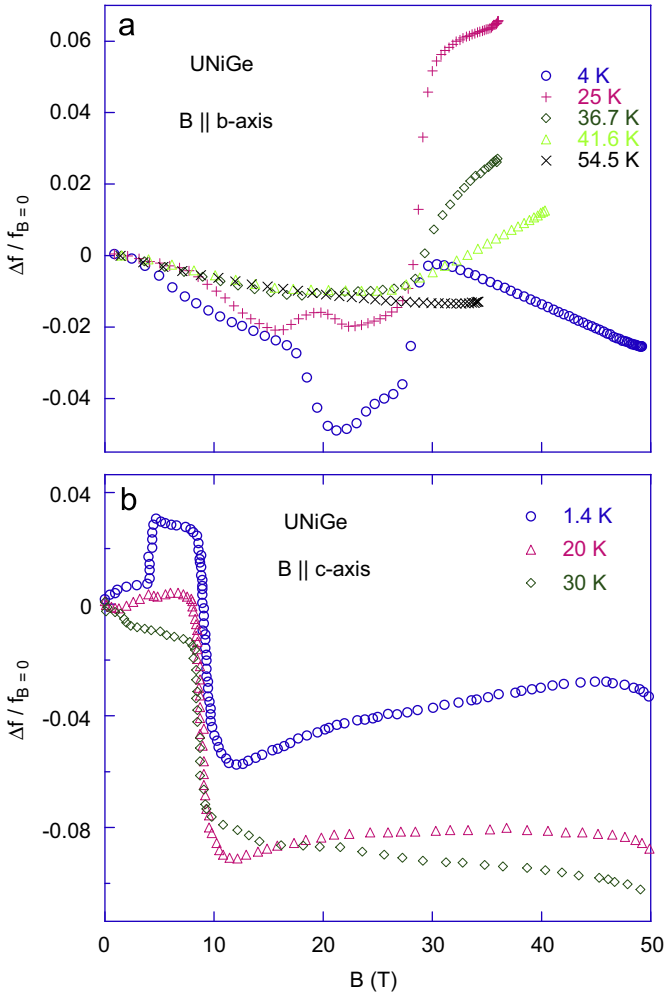

Fig. 9. Field dependence of the relative frequency shift $\Delta f/f_{B=0}$ of the tank-circuit oscillations for UNiGe at various temperatures with magnetic fields applied along (a) the *b*-axis and (b) the *c*-axis.

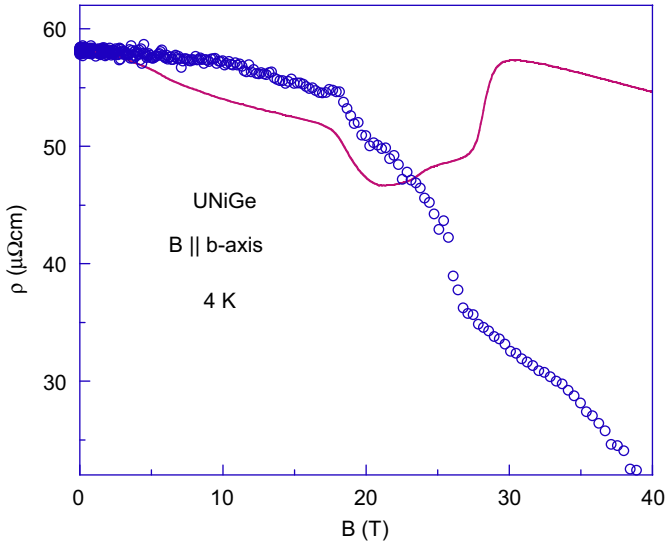

Fig. 10. Field dependence of the electrical resistivity of the UNiGe at 5 K, with B || *b*-axis. Open circles represent our measured resistivity data. The solid line represents the calculated resistivity based on our frequency shift measurements.

geometrical factors, the effective radius of the coil, the effective sample radius, sample shape, filling factor, initial frequency at $B=0$, and the maximal changes in the frequency shifts [7].

Taking the anomalies for the relative frequency shift of the tank circuit $\Delta f/f_{B=0}$ and the magnetoresistance $\Delta\rho/f\rho_{B=0}$ for UNiGe we extracted the transition field for $B\|b$-axis and for $B\|c$-axis. The extracted data were included in previously published B–T phase diagrams and the results are shown in Fig. 11. The B–T phase diagrams contain our results and the previously published results from bulk magnetic and neutron-diffraction studies [38]. Overall, the phase boundaries are in reasonable agreement with the previously reported phase boundaries [38,41]. However, for $B\|b$-axis, there are additional transition fields at higher values at the boundaries between the field-induced uncompensated antiferromagnetic and the ferromagnetic phases. At this point, we do not know if this desecration is due to a new real phase as indicated by our RF results, due to sample missorientation or due

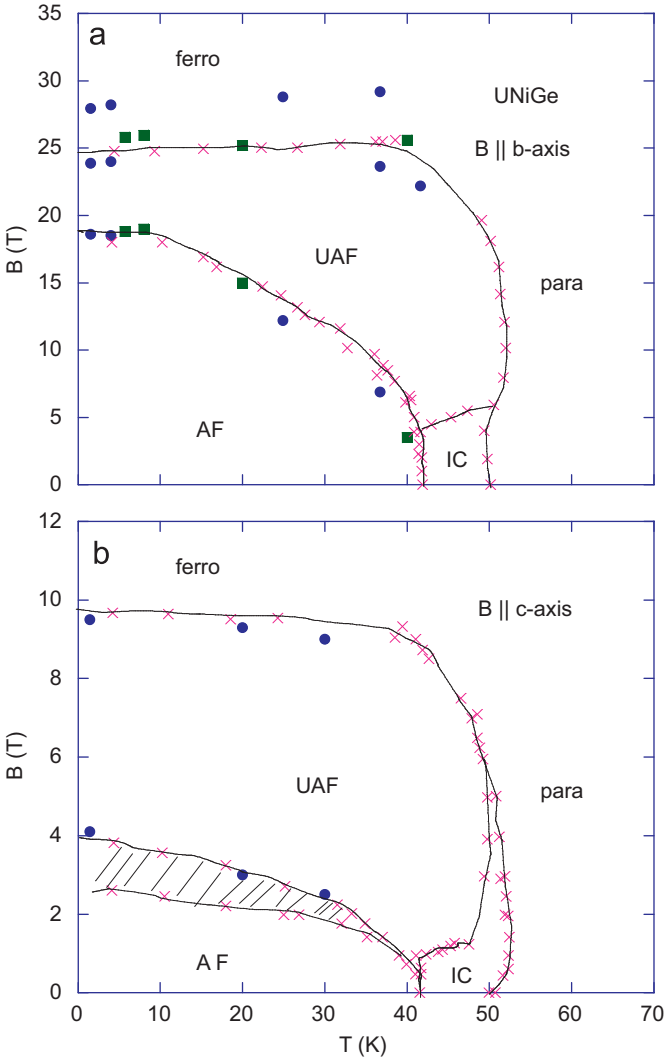

Fig. 11. Magnetic phase diagram of UNiGe for fields applied (a) along the *b*-axis and (b) along the *c*-axis. Solid circles are taken from the anomalies of the relative frequency shift $\Delta f/f_{B=0}$of the tank circuit, solid squares are taken from the anomalies of the relative magnetoresistance $\Delta\rho/\rho(B=0)$ measured by us, and crosses represent the previously published magnetoresistance data [38]. The magnetic phases are labeled incommensurate 'IC' with $q\approx(0,\delta,\delta)$, the field-induced uncompensated antiferromagnet 'UAF' with $q=(0,1/3,1/3)$, the antiferromagnetic ground state 'AF' with $q=(0,1/2,1/2)$, phase, the field-induced ferromagnetically-aligned phase 'ferro', and the paramagnetic phase 'para'. The shaded area in (b) represents a region where hysteresis effects occur. Lines are guides to the eye.

to purely electric effects. Since the boundaries for this phase are taken from the anomalies in the frequency shift measurements and as we discussed before, the frequency shift is sensitive to both the dielectric and magnetic properties of the material. Here, we may speculate and suggest that these anomalies in the frequency shifts could be purely electric in origin.

4. Conclusion

In conclusion, we performed RF skin-depth measurements of antiferromagnetic UNiX compounds (X = Al, Ga, Ge) in magnetic fields up to 60 T applied along different crystallographic directions for temperatures between 1.4 and ~60 K. In most cases, there is a direct correspondence between the features in RF skin depth and magnetoresistance, i.e. the RF skin depth mirrors the magnetoresistance and metamagnetic transitions accompanied by drastic changes in both $\Delta f/f_{B=0}$ and $\Delta\rho/\rho_{B=0}$. This is indicative that both properties can be interpreted in terms of Fermi surface gapping due to the formation of magnetic superzones and/or due to spin-dependent scattering [10].

For UNiGe, however, we find a marked deviation from this behavior with $B\|b$-axis. We find an increase in $\Delta f/f_{B=0}$ at 24 and 28 T but a decrease in $\Delta\rho/\rho_{B=0}$ at ~26 T. The transition at 28 T found in the frequency shift has not been reported before. The different behaviors of $\Delta f/f_{B=0}$ and $\Delta\rho/\rho_{B=0}$ are understood knowing that the frequency shift is sensitive to both the dielectric and magnetic properties of the material. For all the three compounds, UNiAl, UNiGa and UNiGe, the anomalies in $\Delta f/f_{B=0}$ corroborate the previously reported B–T phase diagrams for fields applied along the different crystallographic directions.

Acknowledgements

The work was supported by a grant from NSF (Grant no: DMR-0804032). The NSF, the US Department of Energy and the State of Florida supported the work at the NHMFL, Los Alamos facility. The Hashemite University provided partial support for this work.

References

[1] V. Sechovsky, L. Havela, in: K.H.J. Buschow, (Ed.), Handbook of Magnetic Materials, Vol. 11, Amsterdam, 1998.
[2] V. Sechovsky, L. Havela, in: E.P. Wohlfarth, K.H.J. Buschow (Eds.), Ferromagnetic Materials, Vol. 4, North-Holland, Amsterdam, 1988.
[3] V. Sechovsky, L. Havela, P. Nozar, E. Brück, F.R. de Boer, A.A. Menovsky, K.H.J. Buschow, A.V. Andreev, Physica B 163 (1990) 103.
[4] K.H.J. Buschow, E. Brück, R.G. van Wierst, F.R. de Boor, L. Havela, V. Sechovsky, P. Nozar, E. Sugiura, M. Ono, M. Date, A. Yamagishi, J. Appl. Phys. 67 (1990) 5216.
[5] R.A. Robinson, A.C. Larson, V. Sechovsky, L. Havela, Y. Kergadallan, H. Nakotte, F.R. de Boer, J. Alloys Compd. 213–314 (1994) 528.
[6] N.W. Ashcroft, N. D Mermin, Solid State Physics, Saunders College Publishing, Fort Worth, 1976.
[7] C.H. Mielke, J. Singleton, M.S. Nam, N. Harrison, C.C. Agosta, B. Fravel, L.K. Montgomery, J. Phys.: Condens. Matter 13 (2001) 8325 (and references therein).
[8] E. Ohmichi, E. Komatsu, T. Osada, Rev. Sci. Instrum. 75 (6) (2004) 2094.
[9] C.H. Mielke, J. Singleton, M.S. Nam, N. Harrison, C.C. Agosta, B. Fravel, L.K. Montgomery, Nature (2008).
[10] A.M. Alsmadi, S. Alyones, C.H. Mielke, R.D. McDonald, V. Zapf, M.M. Altarawneh, A. Lacerda, S. Chang, S. Adak, K. Kothapalli, H. Nakotte, J. Appl. Phys. 105 (2009) 07E108.
[11] C.T. van Degrift, Rev. Sci. Instrum. 46 (6) (1975) 599.
[12] L. Havela, V. Sechovsky, P. Nozar, E. Brück, F.R. de Boer, J.C.P. Klaasse, A.A. Menovsky, J.M. Fournier, M. Wulff, E. Sugiura, M. Ono, M. Date, A. Yamagishi, Physica B 136 (1990) 313.
[13] K. Prokeš, F. Bourdarot, P. Burlet, P. Javorsky, M. Olsovec, V. Sechovsky, E. Brück, F.R. de Boer, A.A. Menovsky, Phys. Rev. B 58 (1998) 2692.
[14] E. Brück, H. Nakotte, F.R. de Boer, P.F. de Chatel, H.P. van der Meulen, J.J.M. Franse, A.A. Menovsky, N.H. Kim-Ngan, L. Havela, V. Sechovsky, J.A.A.J. Perenboom, N.C. Tuan, J. Sebek, Phys. Rev. B 49 (1994) 8852.
[15] V. Sechovsky, K. Prokeš, P. Svoboda, O. Syshchenko, O. Chernyavski, H. Sato, T. Fujita, T. Suzuki, M. Doerr, M. Rotter, M. Loewenhaupt, A. Gukasov, J. Appl. Phys. 89 (2001) 7639.
[16] V. Sechovsky, L. Havela, L. Neuzil, A.V. Andreev, G. Hilscher, C. Schmitzer, J. Less-Common Met. 121 (1986) 169.
[17] V. Sechovsky, L. Havela, F.R. de Boer, J.J.M. Franse, P.A. Veenhuizen, J. Sebek, J. Stehno, A.V. Andreev, Physica B 142 (1986) 283.
[18] K. Prokeš, T. Fujita, N.V. Mushnikov, S. Hane, T. Tomita, T. Goto, V. Sechovsky, A.V. Andreev, A.A. Menovsky, Phys. Rev. B 59 (1999) 8720.
[19] O. Mikulina, J. Kamarad, A. Lacerda, O. Syshchenko, T. Fujita, K. Prokeš, V. Sechovsky, H. Nakotte, W. Beyerman, A.A. Menovsky, J. Appl. Phys. 87 (2000) 5152.
[20] F. Honda, V. Sechovsky, O. Mikulina, J. Kamarad, A.M. Alsmadi, H. Nakotte, A. Lacerda, Int. J. Mod. Phys. B 16 (2002) 3330.
[21] F. Honda, K. Prokeš, G. Oomi, T. Kagayama, A.V. Andreev, V. Sechovsky, L. Havela, E. Bruck, J. Phys. Soc. Jpn. 66 (1997) 1904.
[22] K. Usami, J. Phys. Soc. Jpn. 45 (1978) 466.
[23] V. Sechovsky, L. Havela, F.R. de Boer, E. Brück, T. Suzuki, S. Ikeda, S. Nishigori, T. Fujita, Physica B 186–188 (1993) 775.
[24] K. Prokeš, E. Brück, F.R. de Boer, M. Mihalik, A. Menovsky, P. Burlet, J.M. Mignot, L. Havela, V. Sechovsky, J. Appl. Phys. 79 (1996) 6396.
[25] A.V. Andreev, L. Havela, V. Sechovsky, R. Kuzel, H. Nakotte, K.H.J. Buschow, J.H.V.J. Brabers, F.R. de Boer, E. Brück, M. Blomber, M. Merisalo, J. Alloys Compd. 224 (1995) 244.
[26] L. Havela, V. Sechovsky, Y. Aoki, Y. Kobayashi, H. Sato, K. Prokeš, M. Mihalik, A.A. Menovsky, J. Appl. Phys. 81 (8) (1997) 5778.
[27] Y. Kobayashi, Y. Aoki, H. Sugawara, H. Sato, V. Sechovsky, L. Havela, K. Prokeš, M. Mihalik, A.A. Menovsky, Phys. Rev. B. 54 (1996) 15330.
[28] F. Honda, K. Prokeš, M. Olšovec, F. Bourdarot, P. Burlet, T. Kagayama, G. Oomi, L. Havela, V. Sechovsky, A.V. Andreev, E. Brück, F.R. de Boer, A.A. Menovsky, M. Mihalik, J. Alloys Compd. 224 (1995) 244.
[29] V. Sechovsky, K. Prokeš, F. Honda, B. Ouladdiaf, J. Kulda, Appl. Phys. A 74 (2002) S834–S836.
[30] V. Sechovsky, L. Havela, K. Prokeš, H. Nakotte, F.R. de Boer, E. Brück, J. Appl. Phys. 271–273 (1998) 495.
[31] R. Troc, V.H. Tran, J. Magn. Magn. Mater. 73 (1988) 389.
[32] A.P. Ramirez, B. Batlogg, E. Bucher, J. Appl. Phys. 61 (1987) 3189.
[33] F. Canepa, P. Manfrinetti, M. Pani, A. Palenzona, J. Alloys Compd. 234 (1996) 225.
[34] K. Prokeš, H. Nakotte, E. Brück, F.R. de Boer, L. Havela, V. Sechovsky, P. Svobada, H. Maletta, IEEE Trans. Magn. 30 (1994) 1214.
[35] A. Purwanto, V. Sechovsky, L. Havela, R.A. Robinson, H. Nakotte, A.C. Larson, K. Prokeš, E. Brück, F.R. de Boer, Phys. Rev. B 53 (1996) 758.
[36] V. Sechovsky, L. Havela, A. Purwanto, A.C. Larson, R.A. Robinson, K. Prokeš, H. Nakotte, E. Brück, F.R. de Boer, P. Svoboda, H. Maletta, M. Winkelmann, J. Alloys Compd. 293–294 (1994) 536.
[37] H. Nakotte, A. Purwanto, R.A. Robinson, Z. Tun, K. Prokeš, A.C. Larson, L. Havela, V. Sechovsky, H. Maletta, Phys. Rev. B 54 (1996) 7201.
[38] H. Nakotte, I.H. Hagmusa, J.C.P. Klaasse, M.S. Torikachvili, A.H. Lacerda, E. Brück, K. Prokeš, F.R. de Boer, Physica B 246–247 (1998) 441.
[39] P.F. de Châtel, K. Prokeš, H. Nakotte, A. Purwanto, V. Sechovsky, L. Havela, E. Brück, R.A. Robinson, F.R. de Boer, J. Magn. Magn. Mater. 177–181 (1998) 785.
[40] S. Chang, C.H. Mielke, M. Bennett, E. Brück, H. Nakotte, Physica B 312–313 (2002) 877.
[41] F.R. de Boer, K. Prokeš H. Nakotte, E. Brück, M. Hilbers, P. Svoboda, V. Sechovsky, L. Havela, H. Maletta, Physica B 201 (1994) 251.